AIP | Journal of Applied Physics

Magnetic structure and magnetodielectric effect of YFe0.5Cr0.5O3

Vidhya G. Nair, A. Das, V. Subramanian, and P. N. Santhosh

Citation: J. Appl. Phys. **113**, 213907 (2013); doi: 10.1063/1.4808459
View online: http://dx.doi.org/10.1063/1.4808459
View Table of Contents: http://jap.aip.org/resource/1/JAPIAU/v113/i21
Published by the AIP Publishing LLC.

Magnetic structure and magnetodielectric effect of $YFe_{0.5}Cr_{0.5}O_3$

Vidhya G. Nair,[1] A. Das,[2] V. Subramanian,[1] and P. N. Santhosh[1,a)]
[1]*Department of Physics, Indian Institute of Technology Madras, Chennai 600036, India*
[2]*Solid State Physics Division, Bhabha Atomic Research Centre, Mumbai 400085, India*

(Received 9 April 2013; accepted 17 May 2013; published online 5 June 2013)

X-ray diffraction studies reveal *Pnma* space group for $YFe_{0.5}Cr_{0.5}O_3$. The Neel temperature for $YFe_{0.5}Cr_{0.5}O_3$ is found to be ~275 K using temperature dependence of magnetization and neutron diffraction studies. The variation of magnetization with applied magnetic field shows a hysteresis loop at 20 K, which depicts a weak ferromagnetic behavior. Rietveld refinement of the neutron diffraction data divulge a canted antiferromagnetic structure ($\Gamma_4 = G_zF_yA_x$) for $YFe_{0.5}Cr_{0.5}O_3$. Dielectric measurement depicts a relaxor like transition (peak at ~507 K for 10 kHz) for $YFe_{0.5}Cr_{0.5}O_3$. An anomaly in the magnetization curve around this transition temperature points the possibility of magnetodielectric effect in $YFe_{0.5}Cr_{0.5}O_3$. Non-Debye type relaxation is observed with activation energy of 0.40 eV at low temperature and 1.01 eV at high temperature. At high temperatures, oxygen ion vacancies are found to contribute to the conduction process in addition to polaron hopping. © *2013 AIP Publishing LLC*. [http://dx.doi.org/10.1063/1.4808459]

I. INTRODUCTION

Multiferroics are materials in which ferroelectricity, magnetism, and ferroelasticity co-exist. Such materials in which ferroelectric and magnetic orderings are coupled have enormous technological applications.[1–3] However, single phase materials possessing multiferroic behavior and magnetoelectric coupling are rare. Perovskites with general formula ABO_3 (A is a rare earth ion or Yttrium and B a transition metal) are a promising class of multiferroics with simple structure and interesting magnetic properties.[4] These materials in general show low magnetic transition temperature and high ferroelectric transition temperature, for example, $YMnO_3$ shows an antiferromagnetic transition around 80 K and a ferroelectric transition around 914 K.[5] Several other examples ($BiMnO_3$ and $BiFeO_3$) are also known.[3,5,6] Doping magnetic transition elements at the B site of the perovskites ($AB_xB'_{1-x}O_3$) may be an effective strategy to enhance their magnetic properties. The structure and physical properties of $AB_xB'_{1-x}O_3$ perovskites depends on the ionic size and charge differences of the B site cations (B and B′).[7]

$YFe_{0.5}Cr_{0.5}O_3$ (YFC) is one such magnetic material with potential application in spintronics.[8] Few reports on the magnetic properties of $YFe_{0.5}Cr_{0.5}O_3$ are available in the literature.[9,10] A recent report on $YFe_{0.5}Cr_{0.5}O_3$ suggests a canted antiferromagnetic structure.[11] $YFeO_3$ has a canted G–type antiferromagnetic structure below the Neel temperature (T_N) ~640 K while $YCrO_3$ possess canted G–type antiferromagnetic structure with T_N ~140 K and a ferroelectric Curie temperature at ~470 K.[12,13] The weak ferromagnetism observed in these compounds results due to the Dzyaloshinsky–Moriya antisymmetric exchange interaction.[14–16] However, a detailed investigation of the magnetic structure and the high temperature dielectric properties seems to be absent for $YFe_{0.5}Cr_{0.5}O_3$.

In the present work, a detailed investigation of the magnetic structure of $YFe_{0.5}Cr_{0.5}O_3$ is carried out by neutron diffraction technique. In addition, temperature dependence of magnetization in low as well as high temperature region is investigated. Dependence of magnetization with respect to applied magnetic field is also reviewed. High temperature dielectric properties of $YFe_{0.5}Cr_{0.5}O_3$ are explored using impedance spectroscopy techniques. The variation of magnetization in the high temperature region is carried out to probe the magnetodielectric effect in the material.

II. EXPERIMENTAL

Polycrystalline samples of YFC are synthesized by the solid state reaction method. Stoichiometric amounts of highly pure Y_2O_3 (99.99%) (preheated at 873 K for 3 h to remove moisture), Fe_2O_3 (99.99%), and Cr_2O_3 (99.9%) are taken and mixed thoroughly using agate pestle-mortar and heated at 1423 K for 12 h in air with intermediate grinding. The calcined powders are then pressed into pellets of 8 mm diameter and 1 mm thickness using polyvinyl alcohol as the binder and are sintered at 1423 K for 6 h.

X-ray diffraction (XRD) studies were performed using PANalytical X'Pert Pro X-ray diffractometer [Cu K_α (λ = 1.5406 Å)] with a step size of 0.01° in the range $10° \leq 2\theta \leq 90°$. Rietveld refinement of the X-ray powder diffraction pattern of YFC was performed using General Structure Analysis System (GSAS).[17] Neutron diffraction data were collected using multi position sensitive detector (PSD) based powder diffractometer (1.2443 Å) at Dhruva reactor, Bhabha Atomic Research Centre between temperatures 6 K and 300 K in steps of 25 K in the angular range $5° \leq 2\theta \leq 100°$. The neutron diffraction pattern was refined using FULLPROF SUITE.[18] Magnetic measurements [zero field cooled (ZFC) and field cooled (FC)] were performed using Vibrating Sample Magnetometer (Lakeshore VSM 7410) in the temperature range 20 K to 300 K in a magnetic field of 0.1 T and 350 K to 900 K in a magnetic field of 0.3 T. For high temperature magnetic measurement (M

a)Author to whom correspondence should be addressed: E-mail address: santhosh@iitm.ac.in. Tel.: +91 044 2257 4882. Fax: +91 044 2257 4852.

vs T), ZFC starts from room temperature and the data were collected during the warming cycle with an applied field of 0.3 T. In the case of FC, the data were collected during the warming cycle after the sample temperature is lowered to room temperature from 900 K in the presence of same magnetic field (0.3 T) used for taking data in the ZFC case. The magnetic field dependence of magnetization is measured in the field range ±2 T at temperatures 20 K and 300 K. The temperature dependence of dielectric permittivity and dielectric loss was measured from 320 K to 630 K in the frequency range 100 Hz to 1 MHz using N4L (PSM1735) NumetriQ phase sensitive multimeter. The polarization-electric field (P-E) measurement was carried out using precision premier II ferroelectric loop tracer (Radiant Technologies, USA) with a maximum field of 40 kV/cm. Thermogravimetric analysis (TGA) was done using TA Instruments (SDT Q600) in the temperature range 400 K to 800 K.

III. RESULTS AND DISCUSSION

A. Structural studies

Figure 1 shows the room temperature Rietveld refinement plot for the X-ray diffraction pattern of YFC. The shifted Chebyschev function was used to refine the background parameters while the peak profile shape was modeled with pseudo-Voigt function. The refinement revealed that the sample possess an orthorhombic structure with *Pnma* space group (same as that for the parent members $YCrO_3$ and $YFeO_3$). The refined lattice parameter and the volume of YFC (at 300 K) are a = 5.5561(1) Å, b = 7.5734(1) Å, c = 5.2669(1) Å, and V = 221.630(2) Å^3, respectively. The low value of the R-factors, $R_{wp} = 2.47\%$, $R_p = 1.88\%$, and the goodness of fit, $\chi^2 = 1.26$ shows better agreement between the observed and calculated diffraction patterns than mentioned in earlier reports.[8,9] Further, yttrium is found to occupy 4c sites and oxygen 4c and 8d sites while the Fe and Cr ions are randomly distributed at the 4b sites.

B. Magnetic properties

The temperature dependence of magnetization (ZFC and FC) at applied fields of 0.1 T is shown in Figure 2. The magnetization versus temperature curve reveals a strong irreversibility between ZFC and FC. The FC magnetization curve shows a maximum at ~70 K and passes below the ZFC curve anomalously at a temperature of ~150 K, reaches a minimum at ~210 K and again crosses the ZFC at the compensation temperature ~240 K.[8] Further, the magnetization data reveal the Neel temperature of ~275 K, which is in agreement with previous reports.[8] Even above 275 K, the ZFC and FC curves does not coincide, which shows that the true paramagnetic regime has not been attained yet which may be due to short range ordering existing in the material.

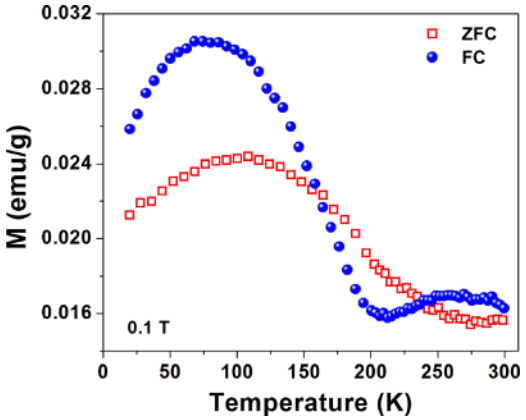

FIG. 2. Magnetization (M) as a function of temperature (at low temperatures) at 0.1 T under ZFC and FC conditions for $YFe_{0.5}Cr_{0.5}O_3$.

Figure 3 shows the field dependence of the magnetization, M-H hysteresis loop of YFC at 20 K and 300 K. The hysteresis loop at 20 K reveals the weak ferromagnetic behavior of the sample. The presence of a loop even at 300 K indicates that the magnetic ordering may be short range. In the M-H curve, the magnetization loop and the linear dependence at high magnetic field can be attributed to the weak ferromagnetism caused from the canting of the moments in the antiferromagnet. The high field part of M (H) curves can be represented as $M = \chi_{AFM}H + \sigma_S$, where, $\chi_{AFM}H$ is the antiferromagnetic contribution and σ_S is the saturation magnetization of the weak ferromagnetism.[10] The weak ferromagnetism or the canted antiferromagnetism results from a small canting of the spins arising due to the

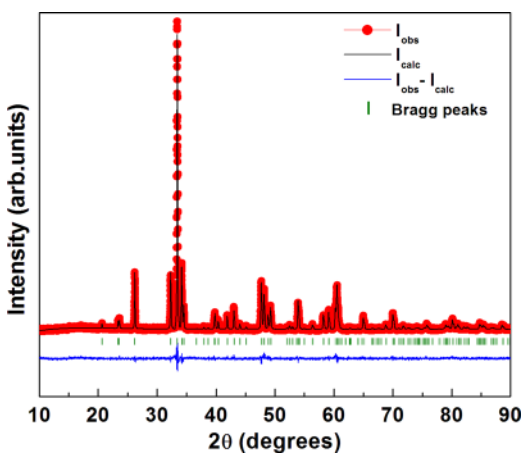

FIG. 1. Rietveld refinement plot (observed (I_{obs}), calculated (I_{calc}), and difference (I_{obs}-I_{calc}) profiles) of X-ray diffraction of $YFe_{0.5}Cr_{0.5}O_3$ at room temperature.

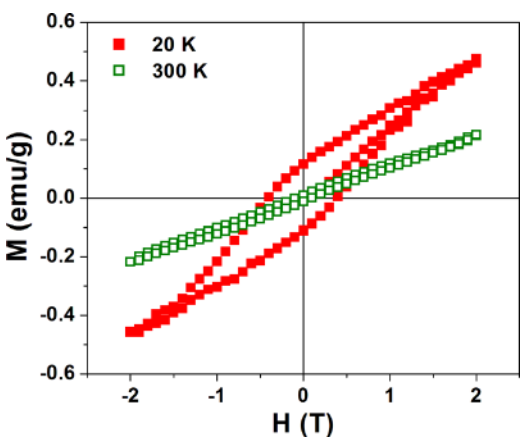

FIG. 3. Isothermal magnetization (M) of $YFe_{0.5}Cr_{0.5}O_3$ at 20 K and 300 K.

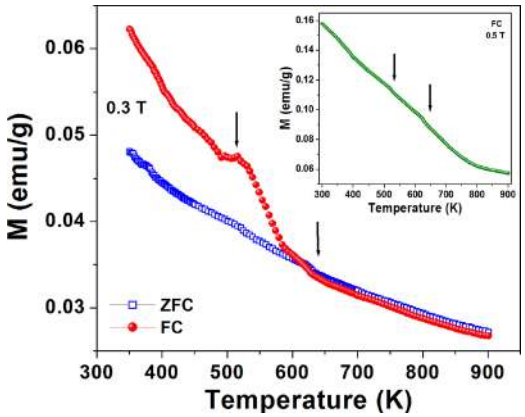

FIG. 4. Magnetization (M) as a function of temperature (at high temperatures) at 0.3 T under ZFC and FC conditions for $YFe_{0.5}Cr_{0.5}O_3$. [Inset shows the FC curve at 0.5 T]. The anomalous behavior marked by the arrows hints towards the magnetodielectric effect in $YFe_{0.5}Cr_{0.5}O_3$.

Dzyaloshinsky–Moriya antisymmetric exchange interaction (DM interaction).[14–16]

The temperature dependence of magnetization at high temperatures from 350 K to 900 K is shown in Figure 4. It clearly shows an anomaly at ~510 K corresponding to the transition temperature in the dielectric measurement (Figure 12(a), ε_r' vs T, Sec. III D) indicating the possibility of magnetodielectric effect in YFC. Another anomaly is observed at ~635 K corresponding to the Neel temperature (640 K) of $YFeO_3$. This reveals that YFC retains the properties of the parent sample establishing that it contains Fe-O-Fe interactions, which may be due to the disordering at B-site in YFC.[11] The magnetic short range ordering predicted above by the M-H curve at 300 K may also be due to ordering of Fe-O-Fe nearest neighbors.

C. Neutron diffraction studies

In order to confirm the magnetic transition temperature and the magnetic structure of YFC, neutron diffraction (ND) measurements were carried out at different temperatures from 6 K to 300 K in steps of 25 K. The room temperature neutron diffraction data does not show any magnetic contribution to the fundamental reflections, which indicates that the magnetic transition is below room temperature confirming the results obtained from the magnetization studies. Rietveld refinement of the neutron diffraction data at 300 K for YFC was performed with the orthorhombic crystal structure in *Pnma* space group (obtained from the Rietveld refinement of X-ray diffraction studies) (Figure 5). Further, the background was fitted by linear interpolation and the peak profile shape is modeled using the pseudo-Voigt function. For 300 K, the refined lattice parameters and the R-factors are given in Table I, while the bond distances, bond angles, and bond valence sums are provided in Table III.

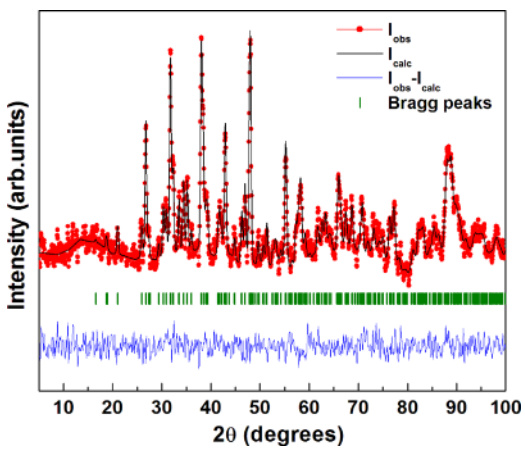

FIG. 5. Rietveld refinement plot (observed (I_{obs}), calculated (I_{calc}), and difference (I_{obs}-I_{calc}) profiles) of Neutron diffraction at 300 K for $YFe_{0.5}Cr_{0.5}O_3$.

TABLE I. Refined lattice parameters and R-factors for neutron diffraction data at 300 K, 250 K, and 6 K for canted G-type antiferromagnetic $YFe_{0.5}Cr_{0.5}O_3$.

T (K)	a (Å)	b (Å)	c (Å)	χ^2	R_{wp} (%)	R_p (%)
300	5.5466(6)	7.5609(8)	5.2588(5)	1.47	7.52	5.86
250	5.5473(4)	7.5592(6)	5.2557(4)	2.56	8.10	6.44
6	5.5456(4)	7.5497(5)	5.2493(3)	2.37	7.99	6.23

In the neutron diffraction data, reflections (110), (011) are observed on cooling below 275 K due to the magnetic ordering of Fe/Cr ions, which is also evident from the temperature dependence of the magnetic reflections (supplementary material, Ref. 31). The pattern numbers mentioned on the left margin of supplementary figure corresponds to the temperatures from 6 K to 275 K in steps of 25 K (pattern number 12 corresponds to 275 K). The magnetic reflections (at $\sim 2\theta = 16^\circ$) gain in intensity starting from ~275 K and depicts maximum intensity at 6 K. The refinement below 300 K was carried out considering both the magnetic and the crystal structures. The magnetic cell is the same as the crystal cell (propagation vector, $k = 0$). The magnetic structure was refined by representation analysis using BASIREPS program.[18]

The neutron diffraction data at 275 K and below are modeled with the irreducible representation $\Gamma_4 = A_xF_yG_z$.[19,20] Refinement of the neutron diffraction data of YFC was carried

TABLE II. Atom positions (x, y, z) and isotropic thermal parameters (B) obtained from refinement of neutron diffraction data of $YFe_{0.5}Cr_{0.5}O_3$ at 300 K, 250 K, and 6 K.

Atom	x	y	z	B (Å^2)
Y	0.0647(6)	0.25	−0.018(1)	0.37(**4**)
	0.0643(6)	0.25	−0.015(1)	0.65(**5**)
	0.0667(4)	0.25	−0.0188(6)	0.26(**3**)
Fe/Cr	0	0	0.5	0.51(**6**)
	0	0	0.5	0.52(**5**)
	0	0	0.5	0.58(**4**)
O1	0.454(1)	0.25	0.106(1)	0.54(**7**)
	0.461(1)	0.25	0.108(1)	0.55(**7**)
	0.4617(7)	0.25	0.1103(8)	0.27(**5**)
O2	0.3042(8)	0.0577(5)	−0.3053(8)	0.37(**4**)
	0.3040(7)	0.0556(4)	−0.3089(7)	0.49(**4**)
	0.3033(5)	0.0569(3)	−0.3069(5)	0.43(**3**)

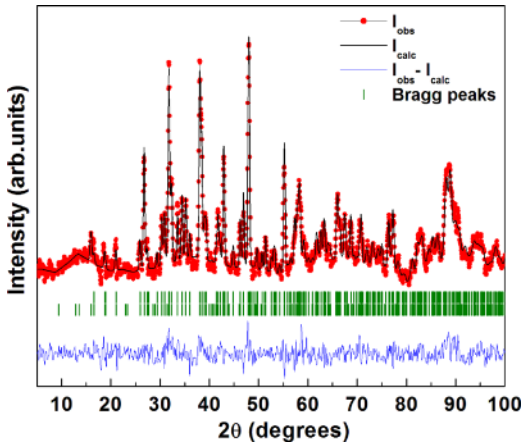

FIG. 6. Rietveld refinement plot (observed (I_{obs}), calculated (I_{calc}), and difference (I_{obs}-I_{calc}) profiles) of Neutron diffraction at 250 K for $YFe_{0.5}Cr_{0.5}O_3$.

out with the $G_zF_yA_x$ spin structure in which the moments are dominantly oriented along the z direction (G_z) with a small canting along the y-direction (F_y) while the spin component along the x-direction (A_x) is found to be negligible. Both the antiferromagnetic (i.e., the G_z component alone) and canted antiferromagnetic structure (i.e., the G_z and F_y component) were considered in the refinement separately in order to get the most appropriate magnetic structure for YFC and also to verify the results obtained from the magnetization measurements.

Figures 6 and 7 shows the Rietveld refinement plot of the neutron diffraction data of YFC at 250 K and 6 K, respectively. The refinement of the neutron data at 6 K depicts a total magnetic moment of $\sim 3.25\,\mu_B$ (expected moment is $4\,\mu_B$), which is equally distributed between Fe and Cr sites. Figure 8 shows the temperature dependence of the magnetic moment, which decreases with increase in temperature (obtained from the refinement). The refined lattice parameter and the respective R-factors at 250 K and 6 K are given in Table I. The magnetic structure obtained from the Rietveld refinement which is a canted G-type antiferromagnet at 6 K is shown in Figure 9.

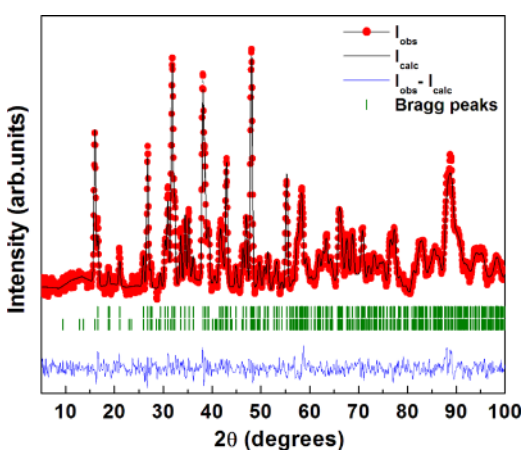

FIG. 7. Rietveld refinement plot (observed (I_{obs}), calculated (I_{calc}), and difference (I_{obs}-I_{calc}) profiles) of Neutron diffraction at 6 K for $YFe_{0.5}Cr_{0.5}O_3$.

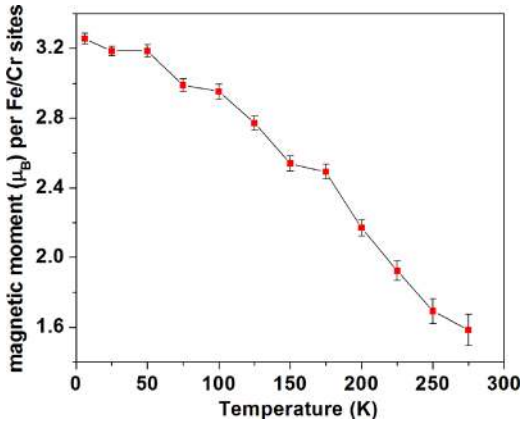

FIG. 8. Temperature dependence of the magnetic moment obtained from Neutron diffraction of $YFe_{0.5}Cr_{0.5}O_3$. (The line is only for visuals not for fitting).

The temperature dependence of the cell volume obtained from the refinement for YFC is shown in Figure 10. The variation of the volume with temperature is fitted using Grüneisen approximation,[21]

$$V(T) = \gamma U(T)/K_0 + V_0, \tag{1}$$

where γ is the Grüneisen parameter, K_0 is the bulk modulus, and V_0 is the volume at T = 0 K. The internal energy U(T) by considering the Debye approximation can be written as

$$U(T) = 9Nk_BT(T/\Theta_D)^3\int_0^{\Theta_D/T} x^3/(e^x - 1)dx, \tag{2}$$

where N is the number of atoms in the unit cell, k_B is the Boltzmann constant, and Θ_D is the Debye temperature. The solid line in Figure 10 shows the fit for the volume data, the value of Θ_D and V_0 are obtained as 419 K and 219.7 Å^3. The value of Debye temperature lies in the range for $YCrO_3$ and some double perovskites.[22,23] The atom positions and isotropic thermal parameters of YFC at 300 K, 250 K, and 6 K are given in Table II while the bond distances, bond angles, and the bond valence sums (BVS) are given in Table III. The

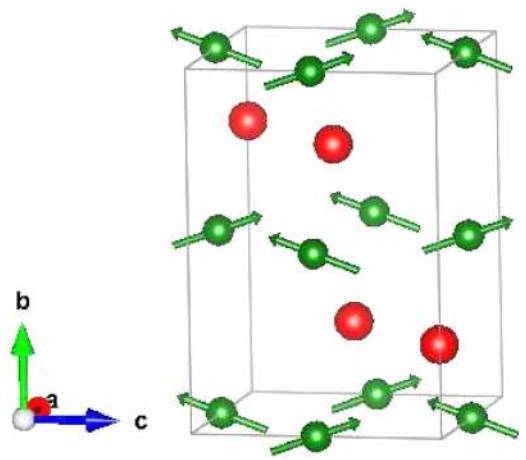

FIG. 9. Magnetic structure at 6 K (Γ_4) obtained from refinement of Neutron diffraction of $YFe_{0.5}Cr_{0.5}O_3$ (yttrium ions are shown as red spheres and Fe/Cr ions as green spheres with spin direction. Oxygen ions are not shown).

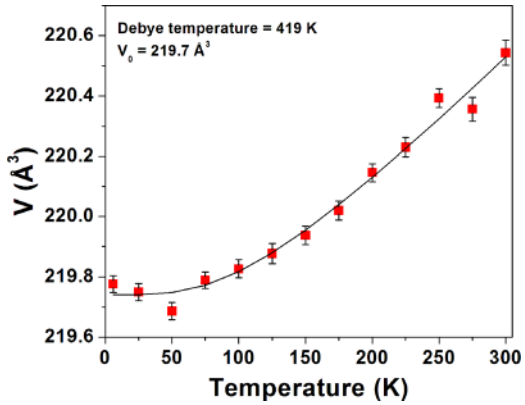

FIG. 10. Temperature dependence of volume (V) obtained from refinement of Neutron diffraction of $YFe_{0.5}Cr_{0.5}O_3$ (The solid line shows the fit with Grüneisen approximation).

bond distances and bond valence sums indicate that both Fe and Cr ions are in 3+ states.

From the neutron diffraction analysis, it can be concluded that canted G-type antiferromagnetic structure is the most suitable structure for YFC at all temperatures which is consistent with the magnetization data. The small loop in the field dependence of magnetization data signifies the occurrence of weak ferromagnetic and antiferromagnetic components in the sample. The neutron diffraction data show a canted G-type antiferromagnetic structure for YFC further

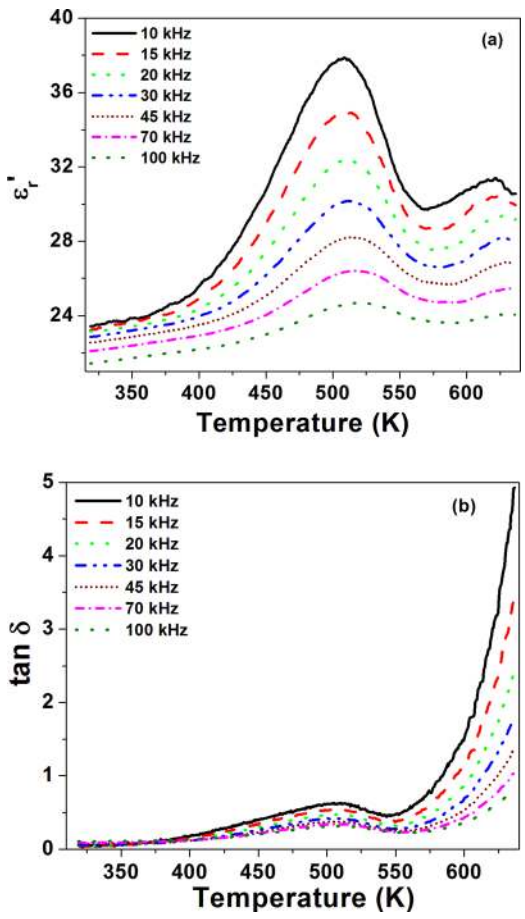

FIG. 11. Temperature dependence of (a) dielectric constant (ε_r'), and (b) dielectric loss (tan δ) of $YFe_{0.5}Cr_{0.5}O_3$ at different frequencies.

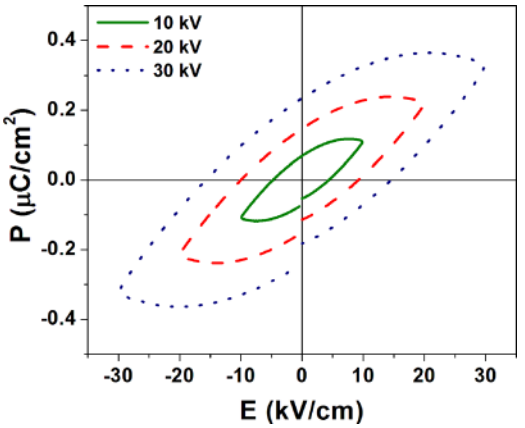

FIG. 12. PE hysteresis loop of $YFe_{0.5}Cr_{0.5}O_3$ at room temperature.

confirming the above findings. The weak ferromagnetism combined with the antiferromagnetism is originated from the effect of antisymmetric DM interactions leading to canting in YFC. Recently, it is reported both experimentally and theoretically that $YFe_{1-x}Cr_xO_3$ shows weak ferromagnetism and magnetization reversal[24] due to DM interactions, which support the canted G-type antiferromagnetic structure as more suitable for YFC.

D. Dielectric properties

The temperature dependence of the real part of dielectric constant (ε_r') and dielectric loss (tan δ) of YFC are shown in Figures 11(a) and 11(b). A diffused ferroelectric transition is observed ~507 K at a frequency of 10 kHz. The dielectric maxima shift to higher temperatures with increase in frequency indicating a relaxor like behavior and this can be attributed to the disordered nature arising from the random distribution of Fe^{3+} and Cr^{3+} ions at the B site.[25] YFC depicted a dielectric constant of ~23 near room temperature, which increases to a maximum value of ~38 as the temperature increases for 10 kHz. Further, as the frequency increases, the dielectric constant maximum decreases. The

TABLE III. Bond distances (Å), bond angles (°), and bond valence sums (BVS) obtained from refinement of neutron diffraction data of $YFe_{0.5}Cr_{0.5}O_3$ at 300 K, 250 K, and 6 K.

	300 K	250 K	6 K
Y-O1	2.2582(2)	2.2947(1)	2.2929(1)
	2.2530(2)	2.2168(1)	2.2216(1)
Y-O2	2.4800(1) x 2	2.5105(1) x 2	2.4770(1) x 2
	2.2493(1) x 2	2.2569(1) x 2	2.2574(1) x 2
	2.6834(2) x 2	2.6552(1) x 2	2.6691(1) x 2
Fe/Cr-O1	1.9875(1) x 2	1.9854(1) x 2	1.9857(1) x 2
Fe/Cr-O2	2.0214(1) x 2	2.0073(1) x 2	2.0104(1) x 2
	1.9866(1) x 2	1.9987(1) x 2	1.9922(1) x 2
Fe/Cr-O1-Fe/Cr	143.99(2)	144.29(1)	143.79(1)
Fe/Cr-O2-Fe/Cr	144.91(1)	145.01(1)	145.06(1)
BVS (Y)	3.036	3.000	3.030
BVS (Fe)	3.143	3.153	3.162
BVS (Cr)	2.860	2.868	2.877
BVS (O1)	2.085	2.096	2.090
BVS (O2)	1.976	1.957	1.980

dielectric loss increases significantly above 570 K due to enhanced electronic motion and dc conductivity of oxygen ions due to the generation of oxygen ion vacancies, which is further confirmed from the calculation of activation energy. An anomaly is observed at ~630 K in the temperature dependence of the dielectric constant corresponding to the magnetic transition temperature of $YFeO_3$. The signature of this magnetic transition is visible in the high temperature magnetization data (Figure 4). The dielectric anomaly ~630 K, corresponding to the T_N of $YFeO_3$, shows the possibility of observing magnetodielectric effect. The room temperature P-E measurement shows a hysteresis loop at different applied electric field, shown in Figure 12. YFC exhibits a weak ferroelectric behavior at room temperature with a remanent polarization of $P_r = 0.23\ \mu C/cm^2$ and a coercive field of $E_c = 15$ kV/cm at 30 kV/cm.

E. Impedance studies

The Cole-Cole plot for YFC is shown in Figure 13. The real (Z′) and imaginary (Z″) part of impedance (Z) are obtained using the relations, $Z' = |Z|\cos\theta$ and $Z'' = -|Z|\sin\theta$. A single depressed semicircle is observed in the Cole-Cole plot (with its center below the real axis) indicating a non-Debye relaxation. Any contributions from the grain boundary or interfacial effect to the dielectric constant are ruled out due to the presence of a single semicircle in the Cole-Cole plot. Hence, the sole contribution to the dielectric constant comes from the bulk of the material. The depressed semicircular behavior can be modeled using a parallel combination of a resistor (with resistance R) and a constant phase element (CPE). The impedance of the constant phase element is given by the relation

$$Z^* = \frac{1}{A(j\omega)^n}, \tag{3}$$

where A is the admittance, and n is an exponent, $0 \le n \le 1$ (measure of depression in the semicircle), a value of 1 for n is typical for the Debye type relaxation and $n < 1$ indicates the distribution of relaxation time. The Cole-Cole plot was fitted using the equivalent circuit shown in the inset Figure 13. The fitting parameters R, A, and n are given in Table IV. The impedance data for YFC on comparison with $YFeO_3$ and $YCrO_3$ reveal that YFC is more resistive. Further, a single depressed semicircle is observed in the impedance plot for YFC, which is associated with bulk resistance of the sample. Whereas, for $YCrO_3$ and $YFeO_3$, in addition to bulk effect, grain boundary and interface effects can also be observed.[26,27]

TABLE IV. Fitted parameters of $YFe_{0.5}Cr_{0.5}O_3$ from Cole-Cole plot.

Temperature (K)	R (MΩ)	A (S rad^{-n}s^n)	n
473	5.8	1.9×10^{-10}	0.81
523	3.2	9.7×10^{-11}	0.84
573	1.9	4.1×10^{-11}	0.90
623	0.3	4.4×10^{-11}	0.90

Using the resistance values (R), the dc conductivity was calculated using the relation, $\sigma = t/RA$, where t is the thickness of the sample and A is the area of cross section of the sample. Figure 14(a) shows the temperature dependence of dc conductivity, which has been found to follow the small polaron hopping mechanism with an Arrhenius type expression given by[28]

$$\sigma T = \sigma_o \exp\left(-\frac{E_{cond}}{k_B T}\right), \tag{4}$$

where σ_o is the pre-exponential factor, E_{cond} is the activation energy for polaronic conduction, and k_B is the Boltzmann constant. The activation energy can be calculated from the slope of the plot ($\ln\sigma T$ vs $10^3/T$). The conduction process is activated by activation energy (E_{cond}) of 0.40 eV in the low temperature range before the ferroelectric transition (~507 K at 10 kHz); while for the high temperature range, E_{cond} is 1.01 eV. In the low temperature range, the only contribution to the conduction process is due to the small polaron hopping; while in the high temperature zone, doubly ionized oxygen vacancies ($V_o^{\cdot\cdot}$) may also contribute to the conduction

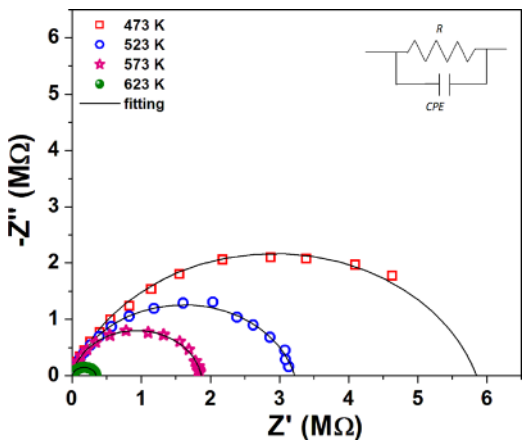

FIG. 13. Cole-Cole plot of $YFe_{0.5}Cr_{0.5}O_3$ at different temperatures. Inset shows the equivalent circuit, which consist of parallel combination of resistor and CPE. The solid line shows fitting with equivalent circuit.

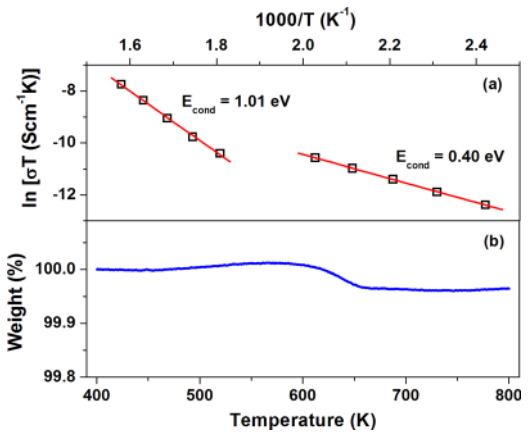

FIG. 14. (a) Temperature dependence of conductivity of $YFe_{0.5}Cr_{0.5}O_3$ fitted with small polaron hopping mechanism (Top panel) and (b) Thermogravimetric analysis of $YFe_{0.5}Cr_{0.5}O_3$ (bottom panel), which shows the oxygen loss.

process.[29] The oxygen loss is also supported by the thermogravimetric analysis (Figure 14(b)), which shows a weight loss around the same temperature range where the contribution from oxygen vacancies to the conduction process begins. The oxygen vacancies ionize and lead to the creation of conducting electrons[30]

$$\left.\begin{aligned} O_o &\leftrightarrow V_o + 1/2O_2 \\ V_o &\leftrightarrow V_o^{\bullet} + e \\ V_o^{\bullet} &\leftrightarrow V_o^{\bullet\bullet} + e \end{aligned}\right\}, \tag{5}$$

where the Kröger-Vink notation of defects is adopted. $V_o^{\bullet}$ and $V_o^{\bullet\bullet}$ represent the oxygen vacancy carrying one and two excess positive charges, respectively.

The frequency dependence of the imaginary part of impedance can be used to analyze the relaxation mechanism in YFC. Figures 15(a) and 15(b) shows the variation of Z″ with frequency in low and high temperature regions. The peak frequency (ω_{max}) corresponds to the relaxation frequency and shifts to higher values with increase in temperature. The variation of relaxation time ($\tau = 1/\omega_{max}$) with temperature is shown in Figure 16. The relaxation time obeys Arrhenius relation with temperature, depicting two relaxation processes with activation energy of 0.45 eV in the low temperature region and 0.99 eV in the high temperature region in tune with the results obtained from temperature dependence of conductivity. As YFC depicted appreciable polaron and oxygen ion conductivities at low and high temperature regimes,

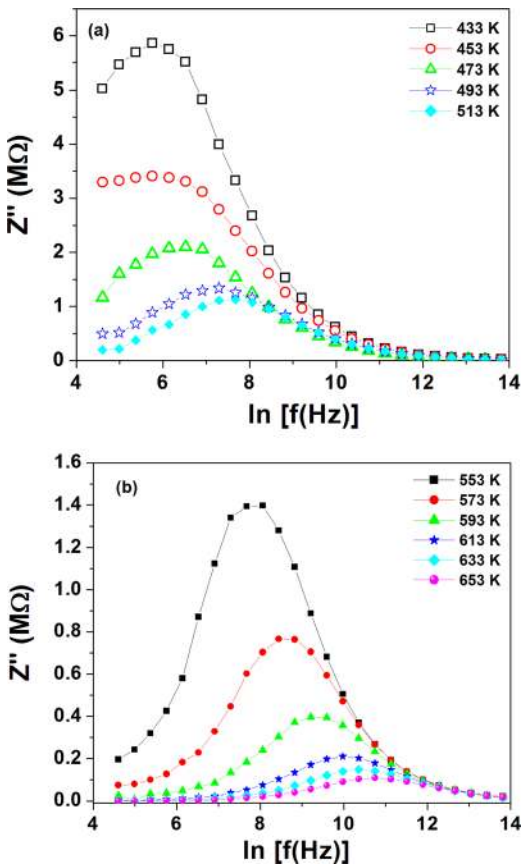

FIG. 15. (a) Variation of Z″ with frequency in (a) low temperature regime, (b) high temperature regime (lines are guide for the eye).

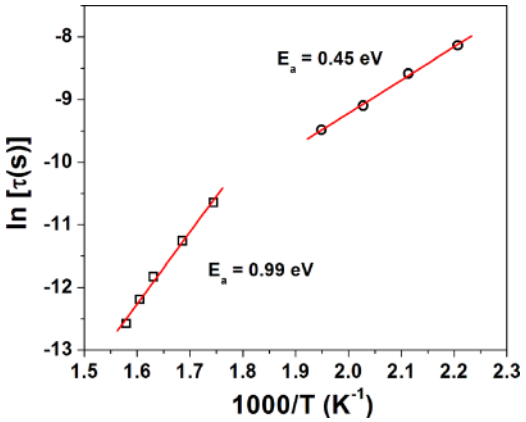

FIG. 16. Temperature dependence of relaxation time (τ) of $YFe_{0.5}Cr_{0.5}O_3$. The solid line shows the fitting with Arrhenius relation.

respectively, it may be a potential candidate as a cathode material in solid oxide fuel cells (SOFCs).

IV. CONCLUSIONS

Polycrystalline $YFe_{0.5}Cr_{0.5}O_3$ is synthesized by solid state reaction method. Rietveld refinement of X-ray diffraction confirms that $YFe_{0.5}Cr_{0.5}O_3$ has an orthorhombic structure with *Pnma* space group. The Neel temperature is ~275 K for $YFe_{0.5}Cr_{0.5}O_3$ as obtained from temperature dependence of magnetization as well as from the neutron diffraction data. Neutron diffraction data confirm the canted antiferromagnetic structure ($\Gamma_4 = G_zF_yA_x$) of $YFe_{0.5}Cr_{0.5}O_3$. Isothermal magnetization shows a hysteresis loop at 20 K, which depicts a weak ferromagnetic behavior that is originated from the Dzyaloshinsky–Moriya antisymmetric exchange interaction. A relaxor like transition is observed for $YFe_{0.5}Cr_{0.5}O_3$ (ε_r' vs T), which can be attributed to the random distribution of Fe^{3+} and Cr^{3+} ions at the B site. Further, an anomaly is observed in the magnetization curve corresponding to this dielectric transition temperature (~507 K), which indicates the possibility of magnetodielectric effect in $YFe_{0.5}Cr_{0.5}O_3$, which needs to be investigated. Impedance spectroscopy reveals the non-Debye type relaxation and gives an activation energy of 0.40 eV at low temperature due to the small polaron hopping and 1.01 eV at high temperature due to doubly ionized oxygen vacancies ($V_o^{\cdot\cdot}$), which also contribute to the conduction process. The activation energy for conduction (1.01 eV and 0.40 eV) and relaxation mechanism (0.99 eV and 0.45 eV) is nearly same, which indicates that the origin is same for conduction and dielectric relaxation.

ACKNOWLEDGMENTS

P.N.S. acknowledge Council of Scientific and Industrial Research (CSIR), India for financial support (Project No. 03(1214)/12/EMR-II). The authors acknowledge BARC, Mumbai for the neutron diffraction measurement and SAIF, IIT Madras for magnetic measurements.

[1]W. Eerenstein, N. D. Mathur, and J. F. Scott, Nature **442**, 759 (2006).
[2]M. P. Singh, K. D. Truong, S. Jandl, and P. Fournier, J. Appl. Phys. **107**, 09D917 (2010).

[3]C. R. Serrao, A. K. Kundu, S. B. Krupanidhi, U. V. Waghmare, and C. N. R. Rao, Phys. Rev. B **72**, 220101(R) (2005).
[4]A. Filippetti and N. A. Hill, Phys. Rev. B **65**, 195120-11 (2002).
[5]C. N. R. Rao and C. R. Serrao, J. Mater. Chem. **17**, 4931 (2007).
[6]A. Moreira dos Santos, A. K. Cheetham, T. Atou, Y. Syono, Y. Yamaguchi, K. Ohoyama, H. Chiba, and C. N. R. Rao, Phys. Rev. B **66**, 064425 (2002).
[7]M. A. Peña and J. L. G. Fierro, Chem. Rev. **101**, 1981 (2001).
[8]J. Mao, Y. Sui, X. Zhang, Y. Su, X. Wang, Z. Liu, Y. Wang, R. Zhu, Y. Wang, W. Liu, and J. Tang, Appl. Phys. Lett. **98**, 192510 (2011).
[9]L. H. Yin, W. H. Song, X. L. Jiao, W. B. Wu, L. J. Li, W. Tang, X. B. Zhu, Z. R. Yang, J. M. Dai, R. L. Zhang, and Y. P. Sun, Solid State Commun. **150**, 1074 (2010).
[10]A. Dahmani, M. Taibi, M. Nogues, J. Aride, E. Loudghiri, and A. Belayachi, Mater. Chem. Phys. **77**, 912 (2003).
[11]B. Rajeswaran, P. Mandal, R. Saha, E. Suard, A. Sundaresan, and C. N. R. Rao, Chem. Mater. **24**, 3591 (2012).
[12]Y. Ma, X. M. Chen, and Y. Q. Lin, J. Appl. Phys. **103**, 124111-5 (2008).
[13]K. Ramesha, A. Llobet, Th. Proffen, C. R. Serrao, and C. N. R. Rao, J. Phys.: Condens. Matter **19**, 102202 (2007).
[14]M. Gorodetsky, S. Shtrikman, Y. Tenenbaum, and D. Treves, Phys. Rev. **181**, 823 (1969).
[15]A. Dahmani, M. Taibi, J. Aride, A. Belayachi, and M. Nogues, Mater. Lett. **54**, 291 (2002).
[16]I. Dzyaloshinsky, J. Phys. Chem. Solids **4**, 241 (1958).
[17]A. C. Larson and R. B. Von Dreele, "General structure analysis system (GSAS)," Los Alamos National Laboratory Report LAUR 86-748 (2004).
[18]J. Rodriguez-Carvajal, *Abstracts of the Satellite Meeting on Powder Diffraction of the XV Congress of the IUCr* (1990), p. 127.
[19]E. F. Bertaut, *Magnetism III* (Academic Press, New York, 1963).
[20]E. Bertaut, J. Phys. IV France **07**, C1–11 (1997).
[21]D. C. Wallace, *Thermodynamics of Crystals* (Dover, New York, 1998).
[22]J. W. Kim, Y. S. Oh, K. S. Suh, Y. D. Park, and K. H. Kim, Thermochim. Acta **455**, 2 (2007).
[23]L. Ortega-San Martin, J. P. Chapman, L. Lezama, J. J. S. Garitaonandia, J. S. Marcos, J. Rodríguez-Fernández, M. I. Arriortua, and T. Rojo, J. Mater. Chem. **16**, 66 (2006).
[24]N. Dasari, P. Mandal, A. Sundaresan, and N. S. Vidhyadhiraja, EPL **99**, 17008 (2012).
[25]A. A. Bokov and Z.-G. Ye, J. Mater. Sci. **41**, 31 (2006).
[26]J. Prado-Gonjal, R. Schmidt, J.-J. Romero, D. Ávila, U. Amador, and E. Morán, Inorg. Chem. **52**, 313 (2013).
[27]Z. X. Cheng, H. Shen, J. Y. Xu, P. Liu, S. J. Zhang, J. L. Wang, X. L. Wang, and S. X. Dou, J. Appl. Phys. **111**, 034103 (2012).
[28]Y. Q. Lin and X. M. Chen, Appl. Phys. Lett. **96**, 142902 (2010).
[29]C. Ang, Z. Yu, and L. E. Cross, Phys. Rev. B **62**, 228 (2000).
[30]X. Sun, C. Wang, G. Wang, C. Lei, T. Li, and L. Liu, J. Am. Ceram. Soc. **96**, 513 (2013).
[31]See supplementary material at http://dx.doi.org/10.1063/1.4808459 for temperature dependence of the magnetic reflections.